Photoelectrons as a tool to evaluate spectral variations in solar EUV irradiance over solar cycle time scales

W.K. Peterson[1], E.N. Stavros[1], P.G. Richards[2], P.C. Chamberlin[1], T.N. Woods[1], S.M. Bailey[3], and S.C. Solomon[4]

[1]Laboratory for Atmospheric and Space Physics, University of Colorado, 1234 Innovation Drive, Boulder, Colorado 80303.
[2]Physics and Astronomy Department, George Mason University, 4400 University Drive, MSN 3F3, Fairfax, Virginia 22030
[3]Bradley Department of Electrical and Computer Engineering, Virginia Tech, 302 Whittemore Hall, Blacksburg, Virginia 24061
[4]National Center for Atmospheric Research, High Altitude Observatory, 1850 Table Mesa Dr., Boulder, Colorado 80307.

Submitted to *J. Geophys. Res.*, April 2009
Revised June 2009
Revised July 2009

Abstract:

There is limited information about the relative magnitude of the spectral variations in the ionizing component of solar irradiance on solar cycle time scales. We found that the TIMED/SEE Version 9 irradiance values predict relatively more ionospheric heating at solar minimum than those from Version 8. These changes have direct impacts on solar cycle timescale variations in ionospheric and thermospheric energy inputs derived from them.

Photoelectron observations from the FAST satellite obtained from 2002 to 2008 are used with solar irradiance data, photoelectron flux models, and models of solar irradiance to examine the solar cycle variations of irradiance in the 4-27 nm range derived from the XPS sensor in the TIMED/SEE instrument suite. Good (± 50%) agreement is found between daily photoelectron observations and model predictions. The largest differences between observed and modeled fluxes are in the 4-10 nm range, where the FAST data show that the SEE Version 9 irradiances are systematically low.

Our analysis suggests that variation on solar cycle time scales in the TIMED/SEE Version 9 and FISM irradiance derived from them are systematically low in the 18-27 nm region. Because of uncertainties in the absolute value of the observed photoelectron fluxes and solar irradiances, differences between observed and modeled photoelectron fluxes are not sufficient to determine more exactly the magnitude of variation on solar cycle time scales of solar irradiance in the 4-27 nm region. These suggestions can be confirmed by higher spectral resolution observations that will be made on the Solar Dynamics Observatory (SDO) mission.

Index Terms:
7537 Solar and stellar variability (1650)
7538 Solar irradiance
7823 Ionization processes (2423)
0358 Thermosphere: energy deposition (3369)

Introduction:

The ionosphere and thermosphere are powered by energy that originates from the Sun in the form of direct solar radiation (irradiance) as well as imposed electric fields and precipitating charged particles. Solar irradiance at X-ray (0.1-10 nm) and extreme ultraviolet (EUV; 10-120 nm) wavelengths produces photoelectrons that heat the thermosphere, drive thermospheric chemistry, and produce dayglow. The solar EUV energy is initially split almost evenly between ions and photoelectrons (Torr et al., 1980). The photoelectrons go on to create secondary ions and emissions, which are important for remote sensing of the thermosphere. Photoelectrons are also responsible for the high thermal electron temperatures in the ionosphere. Only photons with wavelengths below 45 nm are important for producing the observed photoelectron spectrum.

There is limited quantitative information about the relative magnitude of the spectral variations in the ionizing component of solar energy input on solar cycle time scales. Woods et al. [2004] reviewed observations of solar EUV and soft X-ray irradiances prior to the TIMED mission. They examined data from NOAA GOES XRS (0.05- 0.8 nm, Garcia, 1994), Yohkoh SXT (0.2 -3nm, Acton et al., 1999), SNOE SXP (2-20 nm, Bailey et al., 2000, 2001; 2006), SOHO CELLIAS/SEM (26-34 nm, Judge et al., 1998), and rocket observations. They estimated the solar cycle variation in solar irradiance to be a factor of 1.5 to 10 between 65 and 1 nm. They also reported that the integrated irradiance from 1 to 120 nm varied by 30-40% during an active 27-day rotational period and a factor of about 2 over the solar cycle ending in 1996. More recent results from TIMED about solar variability in the EUV range are given by Woods et al. [2005, 2008]. In particular,

73 the TIMED SEE results indicated differences in the absolute values of the irradiances
74 with the previous data sets by more than a factor of 2 at some wavelengths, but the
75 amount of the solar cycle variability during the current cycle is more similar to previous
76 measurements and models of the solar EUV irradiance [Woods et al., 2005].
77 Photoelectrons have been used as a tool to determine the spectral and temporal
78 variations of the solar irradiance driving the Earth's ionosphere. See, for example,
79 Dalgarno et al. 1973. The early comparisons of observed photoelectron spectra with those
80 calculated from models using observed EUV irradiance spectra and atmospheric
81 composition [e.g. Nagy et al., 1977] showed general agreement at energies below about
82 50 eV (above ~19 nm equivalent wavelength), but larger disagreements at higher
83 energies (shorter wavelengths). Richards and Torr [1984] systematically examined the
84 relationship between observed and modeled photoelectron fluxes and concluded that the
85 accepted Heroux and Hinteregger [1978] solar irradiance flux at and below 25 nm was
86 inconsistent with observed photoelectron fluxes, being a factor of 2 too low. Richards et
87 al. [1994a,b] developed the EUVAC model for the temporal and spectral variation of
88 solar irradiance in 37 selected wavelength bands over the region from 5 to 105 nm
89 consistent with photoelectron observations. When higher energy photoelectron
90 observations became available from the Fast Auroral SnapshoT (FAST) satellite [Woods
91 et al., 2003], the EUVAC solar irradiance model was updated to include irradiances from
92 0 to 105 nm at 1 nm resolution [HEUVAC, Richards et al., 2006]. Both EUVAC and
93 HEUVAC are based on solar EUV irradiance measurements from the Atmosphere
94 Explorer program.

95 After the Atmosphere Explorer program ended in 1981 there were no synoptic solar
96 irradiance observations below 45 nm to validate models of solar irradiance used as input
97 to large-scale thermospheric codes. This lack of observations was addressed with the
98 launch of the XUV Photometer System (XPS) sensors aboard NASA's Solar Radiation
99 and Climate Experiment (SORCE, Woods and Rottman, 2005), Thermosphere,
100 Ionosphere, Mesosphere, Energetics, and Dynamics (TIMED, Woods et. al., 1998, 2005)
101 satellites, and the Student Nitric Oxide Explorer (SNOE, Bailey et al. 2000; 2001; 2006).
102 The TIMED/SEE instrument package also includes an EUV grating spectrometer (EGS)
103 with 0.4 nm spectral resolution above 27 nm. The XPS system obtains data below 27 nm
104 from a set of 12 broad band diodes with spectral band passes of 5 to 10 nm covering the
105 spectral range from 0.1 to 35 nm. Because the TIMED XPS filter wheel failed in early
106 2002, SEE now only makes solar measurements with three photometers. The primary
107 channel used in the XPS Level 4 product is a photometer that measures the 0.1-7nm band
108 [Woods et al., 2008]. A calibration program that includes frequent rocket calibration
109 flights maintains long-term accuracy of the observations. Aeronomic calculations of
110 photoelectron fluxes used in large-scale thermospheric models require at least 1 nm
111 resolution. TIMED/SEE scientists have used several solar irradiance spectral models to
112 distribute the 5-10 nm broad band measured irradiances below 27 nm onto 0.1 nm and 1
113 nm resolution data products [Woods et al., 2005, 2008]. Data from TIMED/SEE are
114 currently available for half of a solar cycle from February 9, 2002, which are near solar
115 maximum conditions, to the 2008 measurements reported here taken during solar cycle
116 minimum conditions.

117 In the past few years there has been a re-evaluation of soft X-ray and EUV
118 irradiances commonly used in thermospheric models. See, for example, Solomon and
119 Qian, [2005], Rodgers et al, [2006], and Strickland et al., [2007]. Inconsistencies in
120 observations of airglow and other thermospheric parameters calculated from models
121 based on irradiance data derived from the XPS instruments on TIMED and SORCE
122 suggested a re-evaluation of the algorithms used to distribute irradiance from the broad
123 band observations in the 1-27 nm range to the 1 nm bins used in models [Woods et al.,
124 2008]. Woods and his colleagues noted the simple conversion of the XUV photometer
125 signal into irradiance, in which a static solar spectrum is assumed, overestimates the flare
126 variations by more than a factor of two in specific wavelength bands as compared to the
127 atmospheric response to the flares. To address this deficiency, an improved algorithm
128 using the Chianti spectral model [Landi et al., 2006] was developed to process data from
129 the broad band XUV Photometer System (XPS). The revised irradiance spectra were
130 shown to be consistent with daily variations from the previous simple conversion
131 technique used for XPS. Most importantly, the 1 nm resolution flare variations derived
132 from XPS sensors were reduced by factors of 2 – 4 at wavelengths shorter than 14 nm
133 and are more consistent with the observed atmospheric response to solar flares [Woods et
134 al., 2008].
135 The changes in the reported 1 nm resolution irradiance between 0 and 27 nm
136 introduced in the TIMED/SEE Version 9 data product are significant on the solar cycle
137 time scale. Figure 1 presents the solar irradiance in two broad bands from TIMED/SEE
138 Version 8 (red) and Version 9 (black) from 2002 until mid 2008 covering a significant
139 part of solar cycle 23. The two bands are 0-45 nm which is responsible for most of the

140 photoelectron flux, and the 0-27 nm band where models of the solar spectra are used to
141 distribute observed power in broad XPS bands to the 1 nm resolution required for
142 aeronomic calculations. The green lines on Figure 1 are the irradiance values derived
143 from the HEUVAC model [Richards et al, 2006]. Figure 1 shows that the net effect of the
144 changes between V8 and V9 in the distribution of the XPS power into 1 nm bands below
145 27 nm is to increase the total ionizing solar irradiance, especially later in the mission
146 during solar minimum conditions. The V9 irradiance values predict relatively more
147 ionospheric heating from increased photoionization rates which has direct impacts such
148 as increased satellite drag [e.g. Woodraska, 2007 and Bowman et al., 2008]. To date there
149 has been no independent validation of the magnitude of the variation of the solar
150 irradiance in the 0-27 nm range over solar cycle time scales.
151 Peterson et al., [2008a] have shown that the high sensitivity and energy resolution
152 (i.e. effective high spectral resolution) of the FAST electron spectrometer [Carlson et al.,
153 2001] combined with photoelectron models driven by solar spectra can be used to
154 validate models of solar irradiance variation during a solar flare. The purpose of this
155 paper is to use photoelectron observations from FAST to investigate solar cycle
156 variations in distribution of power from the TIMED/SEE XPS sensor in the TIMED/SEE
157 Version 9 data product shown in Figure 1.
158 Our analysis is based on daily averaged observed and modeled photoelectron fluxes.
159 There are several photoelectron flux models commonly used in thermospheric research.
160 Because photoelectron flux codes do not use the same cross sections and
161 parameterization schemes, we can use the differences in model calculations to provide an
162 estimate of the reliability of the comparisons between photoelectron observations and

163 modeled photoelectron fluxes. Solar irradiance data is sparse, particularly before the 2002
164 launch of TIMED, so investigators rely on several solar irradiance models. Here we limit
165 our analysis to two models of photoelectron flux driven by four different solar irradiance
166 inputs, (one long-term satellite-based measurement and one sounding rocket
167 measurement, as well as two different solar spectral irradiance models). The
168 photoelectron flux models are the Field Line Interhemispheric Plasma (FLIP) model
169 (Richards et al., 2000) and the GLOW model (Solomon et al., 1988; Bailey et al., 2002).
170 These photoelectron models are based on the 2-stream model introduced by Nagy and
171 Banks (1970). Richards and Peterson (2008) used FAST upward and downward fluxes to
172 demonstrate the validity of the 2-stream model. In addition to TIMED/SEE Version 9
173 Level 3 irradiances, we use 0-50 nm solar spectra from HEUVAC [Richards et al., 2006],
174 and the Flare Irradiance Spectral Model (FISM, Chamberlin et al., 2007, 2008). We also
175 use irradiance data obtained at 0.1 nm spectral resolution over the 1-105 nm range on an
176 April 14, 2008 solar minimum rocket calibration flight [Chamberlin et al., 2009; Woods
177 et al., 2009]. The rocket instrument is a prototype of the EUV Variability Experiment
178 (EVE) to be flown on the Solar Dynamics Observatory (SDO). We first examine
179 photoelectron spectra taken on the day of the calibration rocket. We then consider data
180 acquired shortly after TIMED launch in 2002 during solar cycle maximum and during the
181 October-November 2003 interval of intense solar activity. Finally we compare the ratios
182 of FAST photoelectron fluxes between 2002 and 2008 and between 2003 and 2008 with
183 photoelectron fluxes calculated from various photoelectron flux and solar irradiance
184 models on solar cycle time scales.

Data:

The energy-averaged pitch angle spectra in Figure 2 show several horizontal bands equatorward of the auroral oval. The FAST electron spectrometer has a 360^o field of view. Electron pitch angles in the range $0–180^o$ are related to the angle shown as follows: From 0 to 180^o pitch angle equals the angle shown; from 180 to 360^o pitch angle equals 360 minus the angle shown. The widest and most intense band is near pitch angles of 180 degrees, which corresponds to energetic photoelectrons coming up field lines from their source in the ionosphere below. The width of the band of upflowing photoelectrons is determined by the relative strengths of the magnetic field at the satellite and at the top of the ionosphere. The two narrower horizontal bands near 90^o and 270^o pitch angles are produced by photoelectrons generated on spacecraft surfaces that are directed to the electron detectors as they circle the local magnetic field after they are produced. Weaker horizontal bands appear near 0^o and 360^o correspond to down flowing particles in the northern hemisphere. These bands are produced by photoelectrons generated in the magnetically conjugate hemisphere. The band of emissions at about 25 eV seen equatorward of the auroral oval in the top energy time spectrogram is the signature of the well known electron emission lines produced by photoionization of N_2 and O in the ionosphere below the spacecraft by the intense 30.4 nm HeII solar emission line [Doering et al., 1976].

The photoelectron spectra we use to monitor variations in solar irradiance are obtained from FAST electron observations similar to those shown in Figure 2 through a sequence of processing steps that have been described by Woods et al., [2003] and Peterson et al., [2008a]. To increase the signal to noise at higher energies, corresponding

to the highly variable solar emissions below ~27 nm, we start with one-minute averages of the data limited to pitch angles corresponding to ionospheric photoelectrons thus eliminating all spacecraft generated photoelectrons. We then identify and remove one-minute intervals contaminated by auroral electrons. We remove the background signal generated by penetrating radiation as described in Woods et al., [2003]. We determine the spacecraft potential by finding the best fit between the processed spectra and model photoelectron spectra in the region near 60 eV. This region in the spectrum corresponds to a sharp drop in solar irradiance shortward of ~15 nm. To increase the signal to noise ratio further, we consider only daily average photoelectron spectra. Because FAST does not obtain continuous data, the number of usable one-minute spectra per day is determined by orbital position and spacecraft operations.

Photoelectron spectral variations over the solar cycle 23

The focus of this paper is on the relative spectral changes in photoelectron spectra over solar cycle 23. We examined data from August 7, 2002, November 28, 2003, and April 14, 2008. We used daily average observations and daily averages of selected model pair calculations of photoelectron spectra. Model pairs consist of a photoelectron flux code (FLIP or GLOW) and a solar irradiance model. The rocket irradiance spectrum is directly observed at 1 nm or less resolution depending on the wavelength. However, the SEE irradiance below 27 nm uses a model to distribute power measured in broad bands to the 1 nm bins used here. The daily averaged model pair predictions of photoelectron spectra are obtained from model runs for each of the one-minute observed spectra. These daily average photoelectron data had relatively high signal to noise values. April 14, 2008 was chosen because the availability of a rocket calibration spectrum [Chamberlin et al.,

231 2009]. August 7, 2002 was chosen because it was shortly after the TIMED launch and
232 data from an interval including this day has been included in recent publications
233 [Strickland et al., 2004 and Peterson et al., 2008b]. November 28, 2003 was chosen
234 because it occurred shortly after an extend interval of intense solar flare activity.
235 Figure 3 presents the daily average FAST photoelectron spectrum for April 14, 2008
236 as a solid line and * symbols. Fifty-one one-minute spectra obtained at a variety of solar
237 zenith angles (SZA) less than 90^o have been averaged to produce Figure 3. Lee et al.,
238 [1980a, b] and Peterson et al. [2008b] have shown that for SZA's less than 90^o the
239 escaping photoelectron flux is insensitive to the specific value of the SZA. The reason for
240 the independence of SZA is that the escaping photoelectrons are produced high in the
241 thermosphere where there is little attenuation of the solar irradiance. Data quality
242 information and model predictions are also shown in Figure 3. The black dotted line
243 shows the one sigma uncertainty of the observed fluxes based on the instrumental
244 counting rates. The straight line of blue box symbols shows the equivalent flux level of
245 the average penetrating radiation background that has been subtracted. Above about 285
246 eV, which correspond to solar irradiances shortward of ~ 4nm, the instrumental
247 sensitivity and our background subtraction scheme result in flux values that are small
248 compared to the measurement uncertainties. The solar $F_{10.7}$ index for the solar minimum
249 conditions on April 14, 2008 was 69. It is important to note that photoelectrons near 500
250 eV are produced almost exclusively by the Auger ionization of atomic oxygen by a
251 narrow band of photons near 2.2 nm (~560 eV). A substantial proportion of the
252 photoelectrons near 350 eV are created by the Auger ionization of N_2 by photons between
253 2 (620 eV) and 3 nm (413 eV).

In order to use photoelectron spectra to monitor variations in solar irradiance we must use ionospheric models of photoelectron flux based on observed and modeled solar irradiances. The red X symbols are the photoelectron intensities calculated using the solar spectrum measured on the same day from the Chamberlin et al., [2009] calibration rocket as input to the FLIP model. The modeled spectrum reported is the average of calculations made using the SZA, times, and satellite foot point values appropriate for each of the fifty-one observations included in the observational average shown. The agreement between the FLIP photoelectron energy spectrum generated using the rocket solar irradiance spectra is ± 50%, which is good.

Figure 3 also presents the FLIP generated photoelectron spectrum using both the FISM and HEUVAC models as well as a spectrum calculated from the GLOW model using TIMED/SEE Version 9 irradiances. In the absence of solar flares, the FISM and TIMED/SEE irradiances are considered equal to within the published uncertainties.

To more clearly illustrate the agreement between the observations and the FLIP/rocket and the other model pair spectra shown in Figure 3, we have reformatted the data. Figure 4 presents the relative differences between the data and models as a function of the wavelength equivalent of the photoelectron energy. The relative difference is defined as (observations – model) /model. Positive values indicate that the observed fluxes are greater than the modeled fluxes. A value of unity means that the observation is a factor of two larger than the model value. The wavelength equivalent of the photoelectron energy was calculated assuming a 15 eV ionization potential. The data corresponding to photoelectron observations with inadequate signal to noise ratios below 4 nm (above 285 eV) are not included in Figure 4. Compared to the situation before the

277 launch of TIMED, all of the model photoelectron spectra show good agreement with the
278 data; i.e. mostly better than 50%. The comparison is best for the calibration rocket with
279 the prototype EVE instrument.

280 The shape of the photoelectron spectrum obtained on August 7, 2002 is only subtly
281 different from that obtained at solar minimum and shown in Figure 3. Figure 5 presents
282 the relative difference between the August 7 average of 61, one-minute observed FAST
283 photoelectron spectra and spectra calculated from model pairs as a function of the
284 wavelength equivalent of the photoelectron energy. The data corresponding to
285 photoelectron observations with inadequate signal to noise ratios below 2 nm (above 600
286 eV) are not shown. The models and format shown in Figure 5 are the same as those
287 shown in Figure 4. In this case, the comparison is best for the FLIP/HEUVAC model, but
288 we note that the rocket measurements with the EVE instrument were not obtained during
289 that time period.

290 Figure 6 presents the relative difference between the November 28, 2003 average of
291 128, one-minute FAST photoelectron spectra and models as a function of the wavelength
292 equivalent of the photoelectron energy. Signal to noise ratios during this solar maximum
293 day are adequate above 2 nm (below 600 eV). Like the 2002 comparison, the 2003
294 comparison is best for the FLIP/HEUVAC model.

295 Figure 7 compares the observed daily average photoelectron spectra for the selected
296 solar maximum reference days (August 9, 2002 and November 28, 2003) with the
297 spectrum observed at solar minimum on April 14, 2008. Shown as + signs in Figure 7 are
298 the relative difference between the two solar maximum reference photoelectron spectra
299 and that observed at solar minimum as a function of the wavelength equivalent of the

300 photoelectron energy. Data are not reported below 4 nm (285 eV) because of the low
301 signal to noise ratio of the solar minimum photoelectron spectrum in this wavelength
302 (energy) region. The absolute accuracy of the photoelectron observations is estimated at
303 40% [Woods et al., 2003]. The cumulative effect of the 40% uncertainty in the
304 calculation of relative difference is 70%, which is shown for selected energy equivalent
305 wavelengths in Figure 7. Also shown on Figure 7 are the relative differences of
306 photoelectron fluxes calculated using FLIP/FISM, FLIP/HEUVAC, and GLOW/SEE
307 model pairs on these days. The solar ($F_{10.7}$, $F_{10.7A}$) indices for August 7, 2002, November
308 28, 2003, and April 14, 2008 are (136, 168), (168, 140), and (69, 71) respectively, where
309 $F_{10.A}$ is the 81 day running average of F10.7 centered on the current day. The HEUVAC
310 model uses $P = (F_{10.7} + F_{10.7A})/2$ as a wavelength dependent proxy for EUV variations.
311 Thus, despite the differences in daily $F_{10.7}$, we would expect similar solar irradiances for
312 August 7, 2002 and November 28, 2003 in the absence of solar flares. The FAST
313 photoelectron data (crosses) in Figure 7 support this expectation.
314 Figure 7 shows that the solar cycle variation of the FAST photoelectron spectrum has
315 a relative difference less than ~ 0.5 above about 30 nm (less than 25 eV), ~1.5 at 21 nm
316 (42 eV), ~ 0.8 near 16 nm (60 eV), and ~ 8 at 4nm (300 eV), the lowest wavelength
317 (highest energy) for which statistically significant data are available. A relative difference
318 of 1 (8) implies that the solar maximum value is twice (nine times) the solar minimum
319 value. These features are approximately mirrored in the FLIP/FISM and FLIP/HEUVAC
320 and GLOW/SEE model pair comparisons. Below about 6 nm, the FLIP/FISM model pair
321 most closely reproduces the observed variations in the photoelectron spectra over solar
322 cycle 23. Above about 12 nm the FLIP/HEUVAC model pair best matches the

observations. None of the model pairs match the solar cycle variations of the the FAST photoelectron observations well.

Discussion

The comparison between observed and modeled photoelectron spectra presented in Figure 7 is the first attempt to directly verify the applicability of the revised solar model used by Woods et al. [2008] to partition broad band XPS observations below 27 nm from the TIMED/SEE instrument into 1 nm bins over a solar cycle time scale. The TIMED/SEE Version 9 Level 3 irradiance values predict relatively more ionospheric heating from increased photoionization rates over a solar cycle at solar minimum. These changes have direct impacts on ionospheric and thermospheric dynamics calculated from them (see, for example, Solomon and Qian, 2005).

Because high quality photoelectron spectra at energies above ~150 eV (below ~ 7 nm equivalent wavelength) have only recently become available, photoelectron models have not yet been extensively validated in this energy range. We have shown that agreements between FAST and FLIP/HEUVAC photoelectron spectra for August 7, 2002, November 28, 2003, and April 14, 2008 are less than ±0.5 (50%). This is nearly within the observational error estimates of 40% [Woods et al., 2003]. The largest differences are in the 5-15 nm range, where the FLIP/HEUVAC model pair overestimates the observed photoelectron fluxes, especially for the 2008 solar minimum case. The best agreement between predicted and observed photoelectron fluxes was obtained with the rocket calibration spectra at solar minimum (Figure 4).

Agreement with the FLIP/FISM and GLOW/SEE model pairs shown in Figures 4, 5, and 6 is almost as good with relative differences typically less than ±1 (100%). The 5-15

346 nm range, where the differences are near 100%, is dominated by hot coronal emissions
347 especially important during solar flares. Because the FISM and SEE irradiance spectra
348 are nearly identical in the absence of solar flares, the relatively small differences between
349 model pair predictions in this range arise from details of the FLIP and GLOW models.
350 The GLOW/SEE pair also underestimates the observed flux above ~ 30 nm. The general
351 agreement between predictions of the FLIP and GLOW photoelectron flux models below
352 ~ 30 nm gives us confidence that our approach to compare solar irradiance and
353 photoelectron spectra is not significantly limited by details of photoelectron flux models.
354 We defer exploration of the slight differences in the photoelectron flux models below 30
355 nm and the relatively larger differences above 30 nm to a later paper.

356 ## *Wavelength intervals selected for analysis*

357 Here we focus on the region below 27 nm for three reasons. First, this is the region
358 where the spectral shape of the solar irradiance is most uncertain because it is derived
359 from broadband XPS observations. Second, above ~30 nm the photoelectron spectrum is
360 dominated by degraded primary photoelectrons, and third, the wavelength equivalent
361 resolution of the FAST electron spectrometer decreases at longer wavelengths as
362 evidenced by the large spacing of data points in Figures 4, 5, and 6.
363 Woods et al. [2004] estimated the solar cycle variation of irradiance to be a factor of
364 0.5 at 65 nm and up to a factor of 9 at 1 nm. They also reported that, integrated from 1 to
365 120 nm, irradiance varied by about a factor of 2 over solar cycle 22 that ended in 1996.
366 Figure 7 shows that between April 2008 and August 2002 the relative variation of the
367 photoelectron flux varied from 0.5 at 45 nm to about 8 at 4 nm. Furthermore the
368 photoelectron data show a relative maximum variation of ~ 1.5 at 21 nm and a relative

minimum variation of ~ 0.8 at 16 nm. The analysis below is limited by uncertainties in the absolute values of the observed photoelectron fluxes and solar irradiances. The 70% error bars shown in Figure 7 reflect the cumulative effect of the 40% absolute uncertainty in the observed photoelectron fluxes used in the calculation of relative difference.

In order to relate solar cycle variations in the photoelectron spectrum with variations in solar irradiance, we examine variations in solar irradiance in bands relevant to the features identified in Figure 7. Figure 8 shows the integrated irradiance over the indicated wavelength intervals from 2002 until mid 2008. TIMED/SEE Version 8 (red) and 9 (black) Level 3, as well as HEUVAC model (green) data are shown. Table 1 presents the photoelectron energies corresponding to the wavelength bands shown in Figure 8. The FISM model agrees with TIMED/SEE Version 9 Level 3 data, except during solar flares, and is not displayed here. The vertical light blue lines indicate the reference days: August 7, 2002, November 28, 2003, and April 14, 2008. Minimum values in both the variation of irradiance and photoelectron flux over the solar cycle in the 10-16 nm band are seen in Figures 7 and 8. Prominent solar emissions in the 10-16 nm region include the coronal Fe IX, X, and XI emissions. This wavelength range is also associated with the well-known "knee" or sharp fall off in photoelectron fluxes near 60 eV that we use to determine the spacecraft potential.

Figure 8 illustrates the solar cycle effects of the improved XPS radiometric calibration and redistribution of solar irradiance in the TIMED/SEE Version 9 Level 3 data [Woods et al., 2008]. Specifically, irradiance in the 0-l0 nm range was reduced over the solar cycle compared to prior versions. The changes in the 18-27 nm range that were

391 introduced in Version 9 are more complex with a weaker fall-off toward solar minimum
392 compared to Version 8.

393 Figure 9 shows solar spectra from August 7, 2002, November 28, 2003, and April
394 14, 2008 in units of W/m^2-nm. The SEE Version 8 (9) Level 3 spectra are shown in
395 orange (black); HEUVAC spectra are shown in green; FISM spectra are shown in blue;
396 and the April 14, 2008 rocket calibration spectrum is shown in red. The minimum in
397 irradiance near 16 nm (60 eV) is prominent in each spectrum. The differences between
398 the SEE and FISM spectra provide an estimate of the irradiance associated with weak
399 solar flares [Chamberlin et al., 2007, 2008]. Further comparisons of the spectral
400 distribution of solar irradiance over the solar cycle require that we recast the data in
401 Figures 8 and 9 into the relative differences format we used for photoelectron
402 observations.

403 Figure 10 shows the relative difference in the indicated solar spectra relative to those
404 obtained on April 14, 2008 in the format of Figure 7. TIMED/SEE Version 8 data are not
405 available for April 14, 2008 so we only show Version 9 data. Selected data from Figures
406 7, 8, 9, and 10 are given in Tables 2, 3 and 4. Table 2 compares the solar cycle variations
407 of relative differences of observed and modeled photoelectron fluxes for the selected
408 wavelength bands. Table 3 presents variations of solar irradiance models, and Table 4
409 complements the information shown in Figure 8 and presents the relative solar irradiance
410 in the same bands. We note that near 20 nm, the irradiance variation from the HEUVAC
411 model is larger than the TIMED/SEE variation. Figures 9 and 10 confirm the expectation
412 that the solar irradiances for August 7, 2002 and November 28, 2003 are almost the same,

as expected from the near equality of HEUVAC solar flux proxy $(F_{10.7}+F_{10.7A})/2$ for these two days.

Wavelengths below ~12 nm (above 85 eV)

The largest variation in solar irradiance over solar cycle 23 was below 4 nm where Auger ionization of atomic oxygen and molecular nitrogen dominate photoelectron flux [Richards et al., 2006]. We note that the solar minimum FAST photoelectron data are less reliable above 300 eV because of the large background as shown in Figure 1. This problem is reduced at solar maximum because the photoelectron fluxes are larger relative to the background.

Figure 7 and Table 2 show that below ~10 nm the FLIP/FISM model pair best reproduces the observed solar cycle variation of photoelectron fluxes, although there are large uncertainties in the variation of the observed photoelectron fluxes. Figures 4, 5, and 6 show that the FLIP/HEUVAC model pair best reproduces the solar cycle variations of the photoelectron observations longward of ~10 nm. Figure 10 and Table 3 show that the solar cycle variation of irradiance in 0.8-4 and 4-8 nm bands are similar for both the TIMED/SEE Version 9 Level 3 data and HEUVAC model. The differences below 8 nm in Figure 10 between solar cycle variation in the FISM and TIMED/SEE irradiances emphasizes the relative importance of short-term variability associated with small solar flares in this region. Figures 8 and 9 show that the HEUVAC model has relatively more variation in the 4-8 nm band than does the TIMED/SEE Version 9 data. The inconsistency between photoelectron variation below ~10 nm being best reproduced by the FLIP/FISM model pair and daily average photoelectron spectra in the same band being best reproduced by the FLIP/HEUVAC model pair is resolved by considering the

436 data shown in Figures 4, 5, and 6. They show that in the 4-12 nm range the FLIP/FISM
437 model pair underestimates the observed photoelectron fluxes whereas the
438 FLIP/HEUVAC model pair overestimates them. The result is that the FLIP/FISM model
439 pair, which is based on calibrated variations of broad band solar irradiances from XPS
440 over a solar cycle as well as X-ray fluxes from the GOES satellites, best matches
441 observed photoelectron variations while the FLIP/HEUVAC model pair best match
442 individual daily average spectra.

443 Figure 7 shows a gradual increase of solar cycle variation in the observed
444 photoelectron flux from ~1 at 15 nm to ~8 at 4 nm. This variation is approximately
445 reproduced in the photoelectron spectra produced by the various model pairs examined.
446 The equivalent wavelength dependence of the variation, however, does not directly
447 reflect variations in the solar irradiance spectra. As noted by Richards et al. [2006],
448 degraded primary photoelectrons, the so-called cascade population, produce significant
449 ionization. Figure 11 shows as a function of the wavelength equivalent energy the relative
450 importance of directly and indirectly produced electrons. The energy resolution shown in
451 Figure 11 reflects the FAST electron spectrometer response. The FLIP photoelectron
452 code predicts a much more variable equivalent wavelength variation. Figure 11 shows
453 that the contribution from cascade electrons varies significantly as a function of energy
454 and over the solar cycle. The ratios of the photoelectron flux from cascade to that
455 produced directly by photoionization were calculated using the FLIP/HEUVAC model
456 pair. The solid line shows data for April 14, 2008, and the dashed line shows data for
457 August 7, 2002. These calculations are from model runs at 300 (350) km in 2008 (2002).

458 These altitudes have similar neutral densities and correspond to approximate
459 photoelectron escape altitudes for these days.
460 The uncertainties in the data and models presented here are not adequate to
461 unambiguously establish the causes of the differences between the observed and modeled
462 variation in photoelectron spectra in the 1-12 nm range. Figure 11 shows that cascade
463 electrons generated by the O and N_2 Auger photoionization below 4 nm (above 300 eV)
464 account for most of the electrons observed in the 4 to 8 nm band. Another potential
465 contribution to the difference between observed and modeled solar cycle variation below
466 12 nm is that the TIMED/SEE Version 9 Level 3 processing algorithm or FISM model
467 allocates relatively too little power in this region at solar maximum. This is in agreement
468 with the rocket result shown in Figure 4, which indicates more solar irradiance near 10
469 nm than the SEE XPS irradiances. It is also possible that cross sections and other model
470 details in both the GLOW and FLIP models contribute to the disagreement between
471 observed and modeled photoelectron flux variation on solar cycle time scales.

472 ## *Wavelengths from 10 to 16 nm (105 to 60 eV)*

473 Above ~10 nm Table 2 shows that the FLIP/HEUVAC model pair predictions of the
474 variation of photoelectron flux best agree with observations. The variation on solar cycle
475 time scales of photoelectron fluxes and solar irradiances shown in Table 3 in the 10-27
476 nm range are significantly different above and below ~17 nm. In the 10-16 nm range the
477 relative difference of the HEUVAC model solar irradiance over solar cycle time scales is
478 less than the variation of the photoelectron observations; in the 18-27 nm range it is
479 larger than the photoelectron variations. Tables 2 and 3 show that in the 10–27 nm range
480 there is not a simple linear relation between variation in solar irradiance and variation in

photoelectron intensity. Figure 7 shows that the two bands we consider here (10-16 and 18-27 nm) only approximately capture the non-linear relation between variation in solar irradiance and photoelectron flux as a function of wavelength.

Figure 7 shows that the GLOW/SEE and FLIP/FISM model pairs reproduce the observed relative minimum in solar cycle variation of the photoelectron flux near 14 nm. The FLIP/HEUVAC model pair shows this minimum in variation to a lesser degree. Table 3 shows that the variation in HEUVAC irradiance in the 10-16 nm band over the solar cycle is greater than the variation in SEE Level 3 irradiance. Figure 7 and Table 2 show that the photoelectron spectra produced by the FLIP/FISM and GLOW/HEUVAC models pair have lower relative differences in the 10-16 nm band than that of the observations and FLIP/HEUVAC model pairs.

Figure 8 shows that there is relatively little power in the 10-16 nm region over the solar cycle. However, during solar flares irradiance in the 10-16 nm region is relatively more intense. On July 15, 2002, during an X3 class flare, Peterson et al., [2008a] showed the complex spectral and temporal evolution of photoelectron fluxes over the 1-50 nm region. Photoelectron fluxes increased significantly at all energies during the flare. Fluxes in the 60-80 eV range (12 -16 nm equivalent wavelength) had the largest variations in intensity in the interval examined. Photoelectron fluxes less than 60 eV (above 16 nm) had the smallest variation during the solar flare. Photoelectron fluxes derived from the FLIP/FISM model pair best matched the observations in the gradual phase after the flare maximum. However, at the beginning of the flare the FLIP/FISM model pair underestimated the observed fluxes near 60 eV (16 nm).

503 The observations summarized in the two paragraphs above suggest that the relative
504 irradiance distributed in the 10-16 nm range from the broad band XPS observations in the
505 TIMED/SEE Version 9 Level 3 data and the FISM spectra derived from them are too
506 low, especially at solar maximum. The disagreement between observations and models in
507 the 10-16 nm region, however only has a minor effect on the atmosphere because of the
508 low irradiance.

509 ***Wavelengths from 18 to 27 nm (52 to 29 eV)***

510 The data presented in Figures 7, 9, 11, and Tables 2, 3, and 4 suggest that variations
511 on solar cycle time scales in the TIMED/SEE V9 Level 3 irradiances and the FISM
512 irradiances derived from them are about a factor of two lower than the solar cycle
513 variation of FAST photoelectrons in the 18-27 nm band. Figure 11shows a minimum in
514 contributions from the cascade process in this band which demonstrates that the variation
515 of the observed variation in photoelectron flux in the 18-27 nm band comes mostly from
516 variations in solar irradiance. Figure 7 and Table 2 show that the photoelectron spectra
517 produced by the FLIP/FISM and GLOW/SEE models pairs have lower variations in
518 intensity over solar cycle time scales in the 18-27 nm band than those observed and the
519 FLIP/HEUVAC model pair. (However, as shown by Peterson et al. [2008a], during an
520 X3 class flare, photoelectron fluxes derived from the FLIP/FISM model pair best
521 matched the observations in the gradual phase after the flare maximum.) Figures 9, 10,
522 11, and Table 3 show that the variation in HEUVAC irradiance in the 18-27 nm band
523 over the solar cycle is approximately twice that that of the solar cycle variation of the
524 SEE Level 3 irradiance. It is important to note that the SEE Level 3 irradiances include
525 the XPS Level 4 results for the 0-27 nm range and that the XPS Level 4 product is

526 actually a set of spectral models fit to the XPS 0.1-7 nm channel measurement [Woods et
527 al., 2008]. These XPS Level 4 results extend to 40 nm and agree with SEE EGS spectral
528 measurements in the 27-40 nm range to better than 40%, so a difference of ~40% for 18-
529 27 nm range is reasonable.

530 On average, the solar cycle variation between 18 and 27 nm is about a factor of two
531 lower for the TIMED/SEE Version 9 Level 3 data than the FAST photoelectron
532 observations. Table 2 shows that the magnitude of the solar cycle variation in the 18-27
533 nm range observed in the photoelectron fluxes is approximately equal to the variation
534 predicted by the FLIP/HEUVAC model pair. Above 5 nm, the HEUVAC model solar
535 cycle variation is based on the Atmosphere Explorer Satellite irradiances. We base our
536 factor of two estimate on the observation that the ratio of the variation in TIMED/SEE
537 and HEUVAC irradiances in the 18-27 nm band reported in Table 3 is approximately
538 two, which is the same as ratio in variation in photoelectron flux derived from the
539 FLIP/FISM or GLOW/SEE model pair to that given by the FLIP/HEUVAC pair shown
540 in Table 2. Because the best agreement is between observations and model pairs shown at
541 solar minimum in Figure 4, we expect most of the factor of two underestimate of
542 irradiance variation is associated with solar maximum values. Because there is a 40%
543 uncertainty in the absolute values of the photoelectron observations, the uncertainty of
544 the solar cycle variations derived from them is about 70%. Figure 7 shows that at
545 individual wavelengths between 18 and 27 nm, the spectral shapes in photoelectron flux
546 calculated from the FLIP/FISM, GLOW/SEE, and FLIP/HEUVAC model pairs agree
547 with the observed spectral shape. It is unlikely that degradation of the TIMED XPS
548 sensor could be a major factor in the differences noted above. The TIMED XPS and

549 SORCE XPS results are consistent throughout the time period of interest, and the annual
550 calibration rocket flights for XPS have indicated no degradation (to less than 1%) for the
551 XPS primary photometers. The individual comparisons of SEE/XPS results to
552 photoelectron measurements indicate only about 40% differences, for both solar cycle
553 minimum and maximum conditions.

554 Table 4 shows that approximately one third of the TIMED/SEE and HEUVAC
555 ionizing radiation is allocated to the 18-27 nm range over the solar cycle. Solomon and
556 Qian (2005) show that the deposition of solar EUV energy in the thermosphere in 18-27
557 nm region is relatively large from 100 km to over 400 km. If variation over the solar
558 cycle in solar irradiances between 18 and 27 nm is about a factor of two too low in the
559 TIMED/SEE Version 9 Level 3 data, thermospheric models using them are expected to
560 underestimate the solar cycle variation of thermospheric quantities such as density over
561 solar cycle time scales.

562 Finally we note that continuous observations of 0.1 nm resolution solar EUV spectra
563 in the 6-27 nm range and 1.0 nm resolution from 0.1 to 6 nm at a 10-s cadence will soon
564 be available from the SDO EUV Variability Experiment (EVE). These data, rather than
565 the photoelectron data presented here, can be used to improve the algorithm used to
566 distribute power from broadband XPS observations to 1 nm bins. The FAST data
567 presented here and photoelectron data to be obtained from the Canadian ePOP Satellite
568 [Yau et al., 2006] can be used, as they have been here, to test new algorithms to further
569 improve the Level 3 data products derived from TIMED/SEE and SORCE XPS broad
570 band irradiance observations.

Summary and Conclusions:

We found that the TIMED/SEE Version 9 Level 3 irradiance values predict relatively more ionospheric heating at solar minimum than those from Version 8. These changes from the TIMED/SEE Version 8 and earlier Level 3 data can have direct impacts on solar cycle timescale variations in ionospheric and thermospheric energy inputs based on these irradiance values. Photoelectron observations from the FAST satellite obtained from 2002 to 2008 were used along with solar irradiance data, photoelectron flux models, and models of solar irradiance to examine the solar cycle variations of irradiance in the 4-27 nm range derived from the XPS sensor in the TIMED/SEE instrument suite. Our analysis and the conclusions are limited by uncertainties in the absolute magnitude of the observed photoelectron fluxes and solar irradiances.

We examined daily averaged FAST photoelectron spectra from two days at solar maximum and one day at solar minimum. The days at solar maximum were chosen for a lack of impulsive solar flare activity. In contrast to the situation before the launch of TIMED, all of the model photoelectron spectra using SEE and the FISM model derived from SEE irradiances show good (± 100%) agreement with the photoelectron data. The best agreement (± 50%) was with photoelectron spectra calculated from the April 14, 2008 calibration rocket (Figure 4). The best overall agreement was with the photoelectron spectra calculated from the FLIP/HEUVAC model pair. The largest differences are in the 5-15 nm range, where photoelectron spectra derived from the FLIP/FISM and GLOW/SEE model pairs consistently underestimate the observed photoelectron spectra.

We used these data to examine solar cycle variations in distribution of power from the broad band TIMED/SEE XPS sensor in the TIMED/SEE Level 3 Version 9 data

product below 27 nm. The sensitivity of our photoelectron technique is limited by instrumental sensitivity, calibration accuracy, and background counting rates. These factors limit our analysis to equivalent wavelengths above 4 nm (photoelectron energies less than 285 eV). Over the equivalent wavelength region from 4 to 27 nm, the photoelectron data reported here have higher spectral resolution than previously available from the irradiance observations reviewed by Woods et al. [2004] as well as from TIMED/SEE and SORCE. Above 27 nm, higher resolution irradiance spectra are available from the EGS sensor in the TIMED/SEE instrument. Approximately two-thirds of the solar ionizing irradiance power is below 27 nm.

We found that the solar cycle variation of the photoelectron spectrum has a relative maximum difference of ~1.5 at 21 nm (42 eV), a relative minimum difference near 16 nm (60 eV), and a maximum difference of ~ 8 at 4nm (300 eV), the lowest wavelength (highest energy) for which statistically significant data are available. Different pairs of photoelectron flux and solar models best matched the solar cycle variations derived from our observations in different wavelength bands. Below about 6 nm, the FLIP/FISM model pair most closely reproduces the observed variations in the photoelectron spectra over a solar cycle. Above about 12 nm the FLIP/HEUVAC model pair best matches the observations. None of the model pairs captured the observed solar cycle variations well in the 6-12 nm range.

In the 18-27 nm band the data presented here suggest that the TIMED/SEE V9 Level 3 fluxes underestimate the solar cycle variation of solar irradiance by a factor of two. Because of the better agreement between observations and models at solar minimum we expect that most of the difference occurs at solar maximum. Since approximately one-

third of the solar ionizing irradiance is between 18 and 27 nm, we expect that thermospheric models using TIMED/SEE Version 9 Level 3 irradiance will underestimate the variation of thermospheric density over solar cycle time scales.

In the 10-16 nm band the data presented also suggest that the TIMED/SEE V9 L3 fluxes underestimate the solar cycle variation of solar irradiance. This underestimation, however only has a minor effect on the thermosphere because of the low irradiance.

In the 4-8 nm band the data presented here agree well with the predictions of solar cycle variations of photoelectron fluxes from the FLIP/FISM model pair. Auger photoelectrons from O and N_2 below 4 nm (i.e. with energies above 300 eV) produce sufficient secondary photoelectrons to account for a large fraction of difference between the observed and modeled photoelectron distributions.

Comparison of solar irradiance variations and photoelectron fluxes has an uncertainty of about 70%. Consequently, the results presented here are not sufficient to determine the magnitude of variation in solar irradiance in the 4-27 nm region on solar cycle time scales more exactly. Fortunately higher spectral and time resolution EUV spectra will soon be available from the SDO/EVE instrument that can be used for this purpose.

Acknowledgements

WKP thanks Bob Meier, Frank Eparvier, and Juan Fontenla for helpful discussions. We thank the FAST science team for making the data and software available. This research was supported by NASA Grant NNX07B68G and NASA contract NAS5-02140 to the University of Colorado and NASA grants NNX07AN03G and NNX08AF43G to George Mason University.

References:

644 Acton, L., D.C. Weston, and M.E. Bruner (1999). Deriving solar X ray irradiance from
645 Yohkoh observations, *J. Geophys. Res.*, 104, 14,827.
646
647 Bailey, S.M., T.N. Woods, C.A. Barth, S.C. Solomon, R. Korde, and L.R. Canfield
648 (2000). Measurements of the solar soft X-ray irradiance by the Student Nitric Oxide
649 Explorer: First analysis and underflight calibrations, J. Geophys. Res., 105, 27179.
650
651 Bailey, S. M, T. N. Woods, C. A. Barth, and S. C. Solomon, R. Korde, L. R. Canfield
652 (2001), Correction to "Measurements of the Solar Soft X-ray Irradiance by the
653 Student Nitric Oxide Explorer: First Analysis and Underflight Calibrations", *J.*
654 *Geophys. Res*., 106, A8, 15791.
655
656 Bailey, S.M., C.A. Barth, and S.C. Solomon (2002). A model of nitric oxide in the lower
657 thermosphere. J. Geophys. Res. 107, 1205, doi:10.1029/ 2001JA000258.
658
659 Bailey, S. M., T. N. Woods, F. G. Eparvier, and S. C. Solomon (2006), Observations of
660 the Solar Soft X-ray Irradiance by the Student Nitric Oxide Explorer, *Advances*
661 *Space. Res.*, doi:10.1016/j.asr.2005.07.039.
662
663 Bowman, B.B. W.K. Tobiska, and M.J. Kendra (2008), The thermospheric semiannual
664 density response to solar EUV heating, *J. Atmos. And S.T. Phys*., 70, 1482,
665 doi:10.1016/J.jastp.2008-04.020
666
667 Carlson, C. W., et al. (2001), The electron and ion plasma experiment for FAST, *Space*
668 *Sci. Rev.*, 98, 33.
669
670 Chamberlin, P. C., T. N. Woods, and F. G. Eparvier (2007). Flare Irradiance Spectral
671 Model (FISM): Daily component algorithms and results, *Space Weather,* 5, S07005,
672 doi:10.1029/2007SW000316.
673
674 Chamberlin, P. C., T. N. Woods, and F. G. Eparvier (2008). Flare Irradiance Spectral
675 Model (FISM): Flare component algorithms and results, Space Weather, 6, S05001,
676 doi:10.1029/2007SW000372.
677
678 Chamberlin, P. C., T. N. Woods, D. A. Crotser, F. G Eparvier, R. A. Hock, and D. N.
679 Woodraska (2009), Solar Cycle Minimum Measurements of the Solar Extreme
680 Ultraviolet (EUV) Spectral Irradiance on April 14, 2008. *Geophys. Res. Lett*., *36*, in
681 press, doi:10.1029/2008GL037145.
682
683 Dalgarno, A., W.B. Hanson, N.W. Spencer, and E.R. Schmerling (1973). The
684 Atmosphere Explorer mission, *Radio Sci*. 8, 263-266.
685
686 Doering, J.P., W.K. Peterson, C.O. Bostrom, and T.A. Potemra (1976). High resolution
687 daytime photoelectron energy spectra from AE-E, *Geophys. Res. Lett*., 3, 129.
688

689 Garcia, H. (1994). Temperature and emission measure from GOES soft X-ray
690 measurements, *Solar Phys*., 154, 275.
691
692 Heroux, L. and H. Hinteregger (1978). Aeronomical reference spectrum for solar UV
693 below 2000 Å, *J. Geophys. Res*., 83, 5305.
694
695 Judge, D.L, et al. (1998). First solar EUV irradiances obtained from SOHO by the SEM,
696 *Solar Phys*., 177, 161.
697
698 Landi, E., G. Del Zanna, P.R. Young, K.P. Dere, H.E. Mason, and M. Landini, (2006).
699 CHIANTI-An atomic database for emission lines. VII. New data for X-Rays and
700 other improvements. *Astrophys. J. Suppl.* 162, 261.
701
702 Lee, J. S., J. P. Doering, T. A. Potemra, and L. H. Brace, Measurements of the ambient
703 photoelectron spectrum from Atmosphere Explorer, I, AE-E measurements below 300
704 km during solar minimum conditions, *Planet. Space Sci.*, *28,* 947, 1980a.
705
706 Lee, J. S., J. P. Doering, T. A. Potemra, and L. H. Brace, Measurements of the Ambient
707 photoelectron spectrum from Atmosphere Explorer: II. AE-E measurements from
708 300 to 1000 km during solar minimum conditions, Planet. Space Sci., 28, 973-996,
709 1980b.
710
711 Nagy, A. F., and P. M. Banks, Photoelectron fluxes in the ionosphere, *J. Geophys. Res.*,
712 *75*, 6260, 1970.
713 Nagy, A.F., J.P. Doering, W.K. Peterson, M.R. Torr, and P.M. Banks (1977),
714 Comparison between calculated and measured photoelectron fluxes from
715 Atmosphere Explorer C and E, *J. Geophys. Res*., 82, 5099-5102.
716
717 Peterson, W.K., P.C. Chamberlin, T.N. Woods, and P.G. Richards (2008a). Temporal and
718 spectral variations of the photoelectron flux and solar irradiance during an X class
719 solar flare, *Geophys. Res. Lett.*, 35, L12102, doi: 10.1029/2008GL033746.
720
721 Peterson, W.K., T.N. Woods, P.C. Chamberlin, and P.G. Richards (2008b), Photoelectron
722 flux variations observed from the FAST satellite, *Adv. Space Res.* 42, 947-956,
723 doi:10.1016/j.asr.2007.08.038.
724
725 Richards, P.G. and D.G. Torr (1984). An investigation of the consistency of the
726 ionospheric measurements of the photoelectron flux and solar EUV flux, *J. Geophys.*
727 *Res*., 89, 5625-5635.
728
729 Richards, P.G., J.A. Fennelly, and D.G. Torr (1994a). EUVAC: a solar EUV flux model
730 for aeronomic calculations. J. Geophys. Res., 99, 8981-8992.
731
732 Richards, P.G., J.A. Fennelly, and D.G. Torr (1994b). Correction to " EUVAC: a solar
733 EUV flux model for aeronomic calculations", J. Geophys. Res. 99, 13283.

Richards, P. G., et al. (2000), On the relative importance of convection and temperature on the behavior of the ionosphere in North America during January 6– 12, 1997, *J. Geophys. Res.,* 105, 12,763– 12,776.

Richards, P.G., T.N. Woods, and W.K. Peterson (2006). HEUVAC: A new high resolution solar EUV proxy model, *Adv. Space Res.,* 37, 315–322, doi:10.1016/j.asr.2005.06.031

Richards, P. G., and W. K. Peterson (2008), Measured and modeled backscatter of ionospheric photoelectron fluxes, *J. Geophys. Res., 113*, A08321, doi:10.1029/2008JA013092.

Rodgers, E. M., S. M. Bailey, H. P. Warren, T. N. Woods, and F. G. Eparvier (2006), Soft X-ray irradiances during solar flares observed by TIMED-SEE, *J. Geophys. Res.*, 111, A10S13, doi:10.1029/2005JA011505.

Solomon, S.C., P.B. Hays, and V.J. Abreu (1988). The auroral 6300A ˚ emission: observations and modeling. *J. Geophys. Res*. 93, 9867.

Solomon, S. C., S. M. Bailey, and T. N. Woods (2001), Effect of Solar Soft X-Rays on the Lower Ionosphere, *Geophys. Res. Lett.*, *28*(11), 2149–2152.

Solomon, S. C., and L. Qian (2005), Solar extreme-ultraviolet irradiance for general circulation models, *J. Geophys. Res.*, 110, A10306, doi:10.1029/2005JA011160.

Strickland, D. J., et al. (2007), Constraining and validating the Oct/Nov 2003 X-class EUV flare enhancements with observations of FUV dayglow and E-region electron densities, *J. Geophys. Res*., 112, A06313, doi:10.1029/2006JA012074.

Torr, M. R., D. G. Torr, and P. G. Richards (1980), The solar ultraviolet heating efficiency of the midlatitude thermosphere, *Geophys. Res. Lett., 7*, 373-376.

Woodraska, D.N., T.N. Woods, and F.G. Eparvier (2007), Comparison of TIMED satellite drag with Solar EUV Experiment (SEE) Measurements , J. of Spacecraft and Rockets, 44, 1204.

Woods, T., F. Eparvier, S. Bailey, S. C. Solomon, G. Rottman, G. Lawrence, R. Roble, O. R. White, J. Lean, and W. K. Tobiska (1998). TIMED Solar EUV Experiment, SPIE Proc., 3442, 180.

Woods, T. N., S. M. Bailey, W. K. Peterson, S. C. Solomon, H. P. Warren, F. G. Eparvier, H. Garcia, C. W. Carlson, and J. P. McFadden (2003). Solar extreme ultraviolet variability of the X-class flare on 21 April 2002 and the terrestrial photoelectron response, *Space Weather,* 1(1), 1001, doi:10.1029/2003SW000010.

780 Woods, T., L. W. Acton, S. Bailey, F. Eparvier, H. Garcia, D. Judge, J. Lean, D.
781 McMullin, G. Schmidtke, S. C. Solomon, W. K. Tobiska, and H. P. Warren (2004).
782 Solar extreme ultraviolet and x-ray irradiance variations, in Solar Variability and Its
783 Effect on Climate, eds. J. Pap, C. Fröhlich, H. Hudson, J. Kuhn, J. McCormack, G.
784 North, W. Sprig, and S. T. Wu, Geophys. Monograph Series, 141, Wash. DC, 127-
785 140.
786
787 Woods, T. N., F. G. Eparvier, S. M. Bailey, P. C. Chamberlin, J. Lean, G. J. Rottman, S.
788 C. Solomon, W. K. Tobiska, and D. L. Woodraska (2005), Solar EUV Experiment
789 (SEE): Mission overview and first results, J. Geophys. Res., 110, A01312,
790 doi:10.1029/2004JA010765.
791
792 Woods, T.N. and G. Rottman (2005). XUV Photometer System (XPS): Solar variations
793 during the SORCE mission, *Solar Phys*., 230, 375-387.
794
795 Woods, T. N., J. L. Lean, and F. G. Eparvier (2006), The EUV variability experiment
796 (EVE): Science plans and instrument overview, in International Living With a Star
797 (ILWS) Proceedings, Goa, India, edited by N. Gopalswamy and A. Bhattacharyya,
798 pp. 145– 152, Quest, Mumbai, India.
799
800 Woods, T.N., et. al (2008), XUV Photometer System (XPS): Improved solar irradiance
801 algorithm using Chianti spectral models, *Solar Physics*, DOI:10.1007/s1207-008-
802 9196-6s.
803
804 Woods, T.N., et al. (2009). Solar irradiance reference spectra (SIRS) for the 2008 whole
805 heliosphere interval (WHI), *Geophys. Res. Lett*., 36, L36101,
806 doi:10.1029/2008GL036373
807
808 A.W. Yau, H.G. James, and W. Liu (2006). The Canadian Enhanced Polar Outflow Probe
809 (e-POP) mission in ILWS, Adv. Space Res., 38, 1870-1877,
810 doi:10.1016/j.asr.2005.01.05

811

Wavelength and energy bands

Wavelength equivalent (nm)	Photoelectron Energy (eV)
0.8 - 4	285 – 1,500
4 - 8	135 - 285
10 - 16	60 – 105
18 – 27	29 - 52
0.8 – 45	12 – 1,500

Table 1: Photoelectron energies corresponding to the wavelength bands shown in Figures 1 and 8. Rather than 0 nm corresponding to an infinite photoelectron energy we have used 0.8 nm as the lower wavelength limit here.

Relative variation of photoelectron flux over a solar cycle time scale

Wavelength Range (nm)	0.8-4 nm	4-8 nm		10-16 nm		18-27 nm		0.8-27 nm	0.8-45 nm
Interval	Both	August, 2002	November 2003	August, 2002	November 2003	August, 2002	November 2003	Both	Both
Photoelectron Observations	-	4.0	4.4	1.0	1.3	0.9	1.2	-	-
FLIP/FISM	30	3.2	4.1	0.5	0.7	0.4	0.6	5.4	3.3
FLIP/HEUVAC	5.0	2.0	2.0	1.0	1.1	1.1	1.3	1.8	1.3
GLOW/SEE	8.4	2.0	2.1	0.4	0.5	0.3	0.5	1.9	1.3

Table 2. Relative variation of photoelectron observations, FLIP/FISM, FLIP/HEUVAC, and GLOW/SEE. For the 0.8-4, 0.8-27, and 0.8-45 nm bands relative difference reported is the average of those obtained using the August 9, 2002 and November 28, 2003 data and both are relative to the April 14, 2008 data. The average of the relative variation for the two dates are shown for the other bands. Variations less than 0.7 are not considered significant due to uncertainties in the absolute value of the photoelectron flux.

Relative variation in solar irradiance over a solar cycle time scale

Wavelength Range (nm)	0.8-4 nm	4-8 nm		10-16 nm		18-27 nm		0.8-27 nm	0.8-45 nm
Interval	Both	August, 2002	November 2003	August, 2002	November 2003	August, 2002	November 2003	Both	Both
SEE/V9	4.8	1.0	1.1	0.4	0.5	0.7	0.8	0.8	0.9
HEUVAC	5.0	1.4	1.4	0.8	0.7	1.7	1.6	1.5	1.3

Table 3 Relative variation of solar irradiance. SEE/V9 data are from the level 3 data product and do not include the effects of solar flares. For the 0.8-4, 0.8-27, and 0.8-45 nm bands relative difference reported is the average of those obtained using the August 9, 2002 and November 28, 2003 data and both are relative to the Arpil 14, 2008 data.

Relative irradiance power in selected bands

Wavelength Range (nm)	SEE V9 Level 3			HEUVAC			Rocket
	August 2002	November 2003	April 2008	August 2002	November 2003	April 2008	April 2008
0.8-4	7	8	2	5	5	2	3
4-8	6	6	6	10	10	10	6
10-16	3	3	4	4	4	5	4
18-27	28	38	32	35	35	31	30
0.8-27	57	60	63	69	69	64	64
27-45	43	40	37	31	31	36	36
0.8-45	100	100	100	100	100	100	100

Table 4. Relative irradiance power in percent in selected wavelength bands for the three days examined here. See Figure 8 for the irradiance in these bands as a function of time for the SEE and HEUVAC irradiances.

Figures:

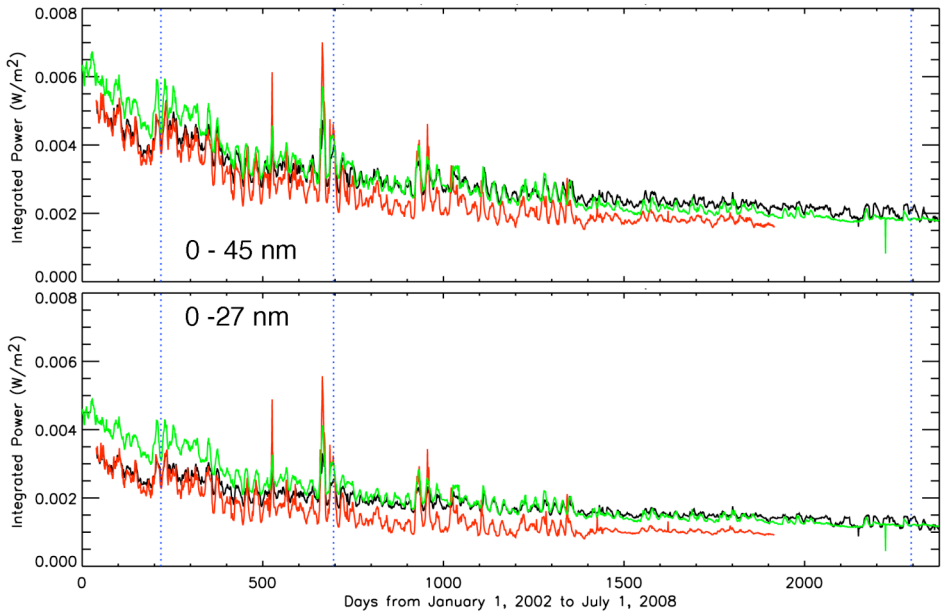

Figure 1: Solar irradiance power in the 0-45 nm (top) and 0-27 nm (bottom) range from January 2002 to mid 2008. Data from the TIMED/SEE Version 8 (9) Level 3 are shown in red (black). HEUVAC [Richards et al., 2006] model output is shown in green. The vertical blue lines mark days were photoelectron observations are compared below. These are August 7, 2002, November 28, 2003, and April 14, 2008.

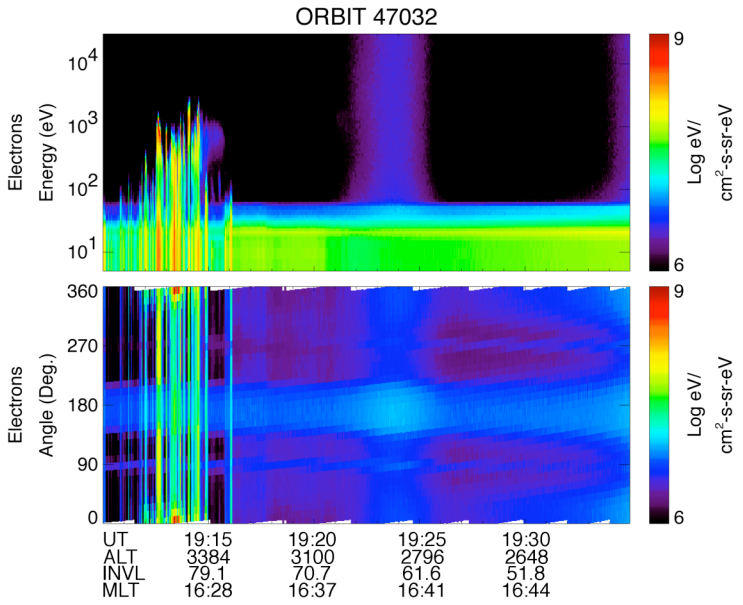

Figure 2 presents an overview of FAST electron data obtained ~3000 km above the ionosphere in the northern hemisphere from 19:05 to 19:35 UT on April 14, 2008, shortly after data from the calibration rocket [Chamberlin et al., 2009] were acquired. The top panel shows electron energy spectra averaged over all pitch angles as a function of time. The bottom panel shows angle spectra averaged over energies from 100 to 12,000 eV as a function of pitch angle. Electron pitch angle in the range 0–180_ is related to the angle shown as follows: From 0 to 180_ pitch angle equals the angle shown; from 180_ to 360_ pitch angle equals 360_ minus the angle shown.. The intensities in units of cm^{-2}-s-sr-eV are encoded using the color bars on the right. The spacecraft is in the polar cap post-noon auroral zone until ~19:17 UT. After this time the spacecraft is on closed magnetic field lines equatorward of the auroral oval. Just before 19:25 UT the satellite passes through the outer radiation belts where a background signal generated by penetrating energetic particles dominates the angle spectra and the energy spectra above ~ 50 eV.

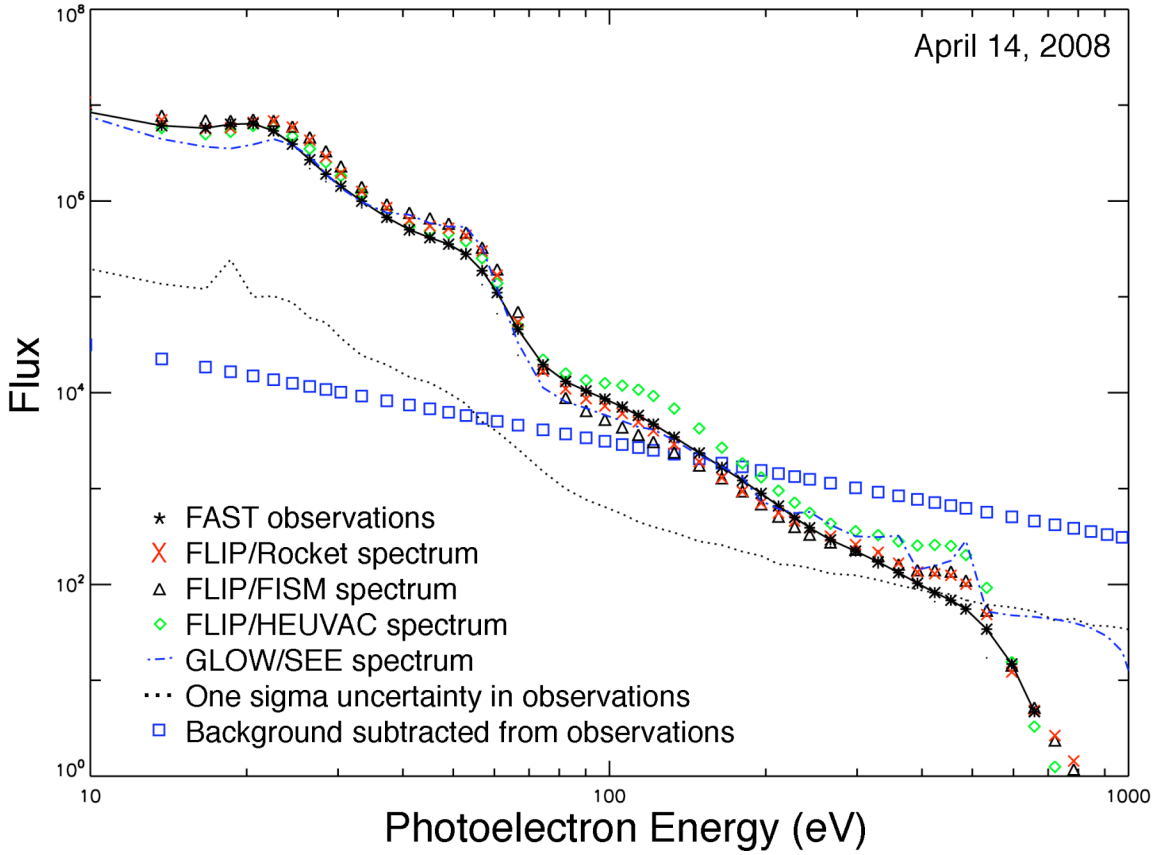

Figure 3: Observed and modeled photoelectron daily average photoelectron fluxes on April 14, 2008 in units of (cm2-s-sr-eV)-1 as a function of energy in eV. Fast observations are shown as a solid line connecting * symbols. The one standard deviation uncertainty in the flux measurement is indicated by the black dotted line; the background from penetrating radiation is shown by blue boxes. Photoelectron fluxes calculated using FLIP model with the 2008 rocket data are shown by red X's, with the FISM solar model by black triangles, and with the HEUVAC solar model by green diamonds. Spectra calculated using the GLOW with the SEE Version 9 fluxes are shown as the dot dash blue line. In the absence of solar flares, the FISM and TIMED/SEE irradiances are expected to be very similar

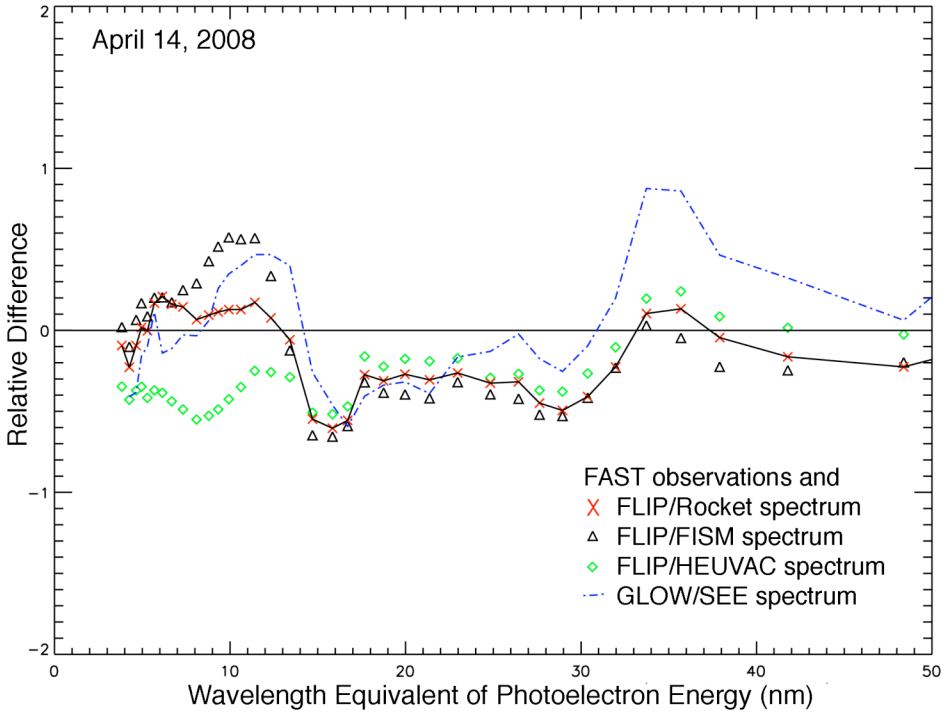

Figure 4: Relative differences between observed and modeled daily average photoelectron fluxes [(Observed – Model)/Model] on April 14, 2008 as a function of the wavelength equivalent of the photoelectron energy. For descriptions of comparisons of the combinations of photoelectron model and solar spectra indicated see text.

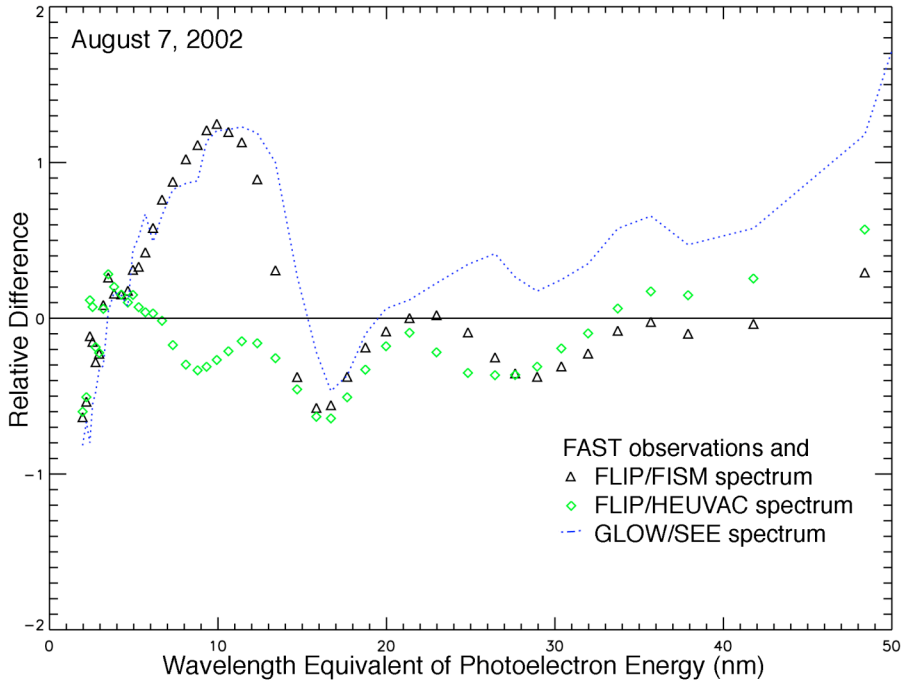

Figure 5: Relative differences between observed and modeled daily average photoelectron fluxes on August 7, 2002 as a function of the wavelength equivalent of the photoelectron energy. For descriptions of comparisons of the combinations of photoelectron model and solar spectra indicated see Figure 4 and text.

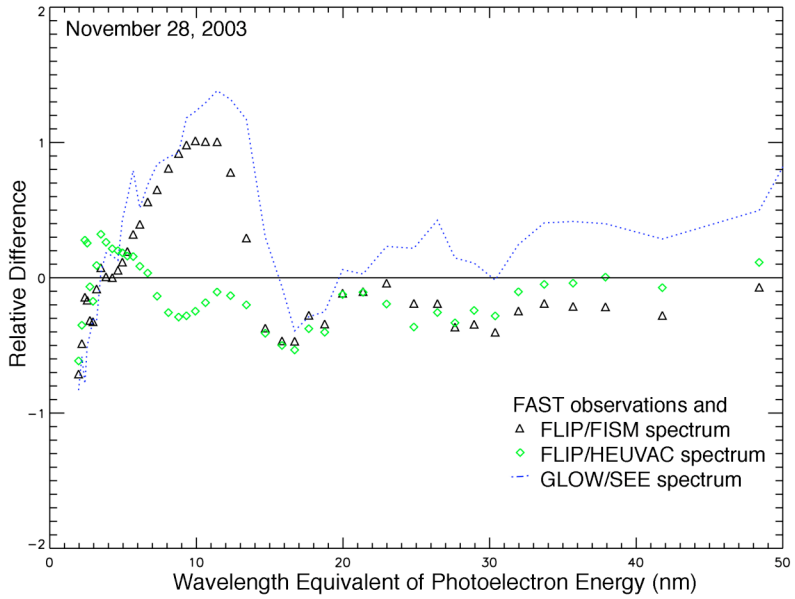

Figure 6: Relative differences between observed and modeled daily average photoelectron fluxes on November 28, 2003 as a function of the wavelength equivalent of the photoelectron energy.

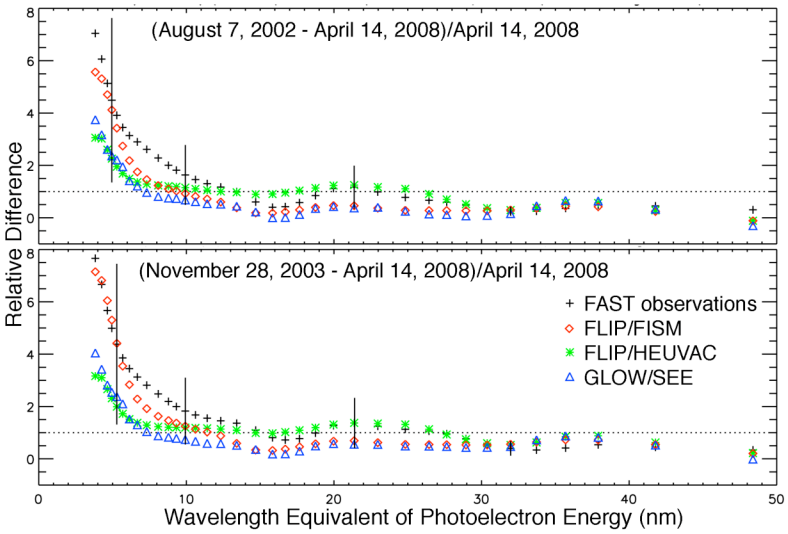

Figure 7: Relative differences between average photoelectron spectra on selected days. Fro a description of the comparisons as a function of the wavelength equivalent of the photoelectron energy see text.

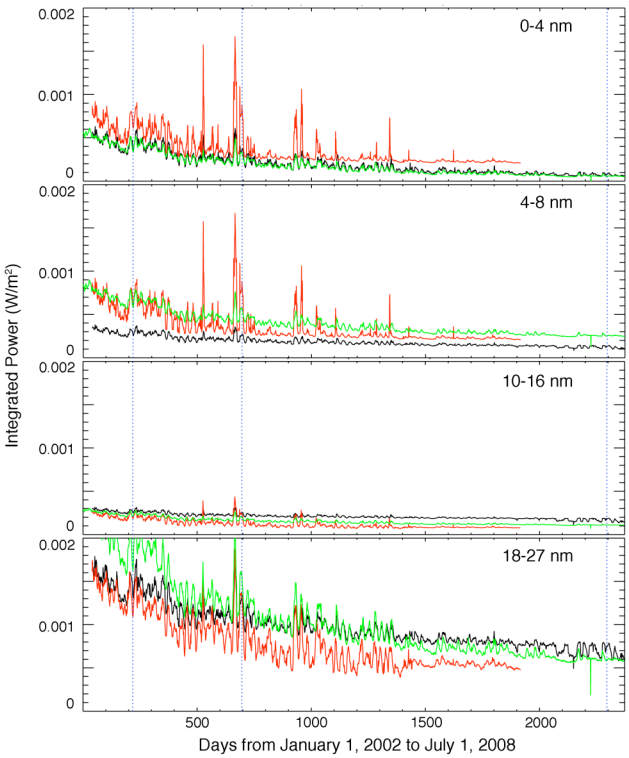

Figure 8: Integrated irradiance over the indicated wavelength intervals from 2002 until mid 2008. TIMED/SEE Version 8 (red) and 9 (black) Level 3, as well as HEUVAC model (green) data are shown. See Figure 1 for irradiance power in the 0-27 and 0-45 nm wavelength intervals. In the absence of solar flares, the FISM and TIMED/SEE Version 9 irradiances are expected to be similar.

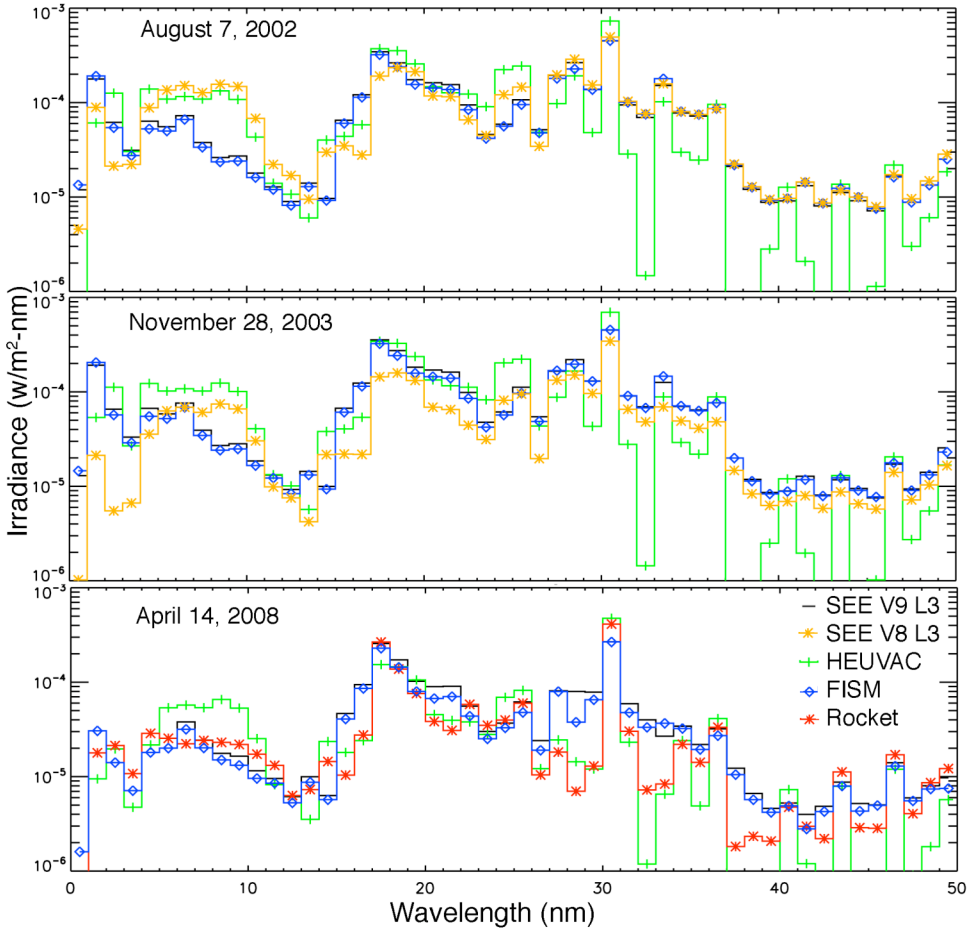

Figure 9: Solar irradiance as a function of wavelength from August 7, 2002, November 28, 2003, and April 14, 2008 in units of W/m^2-nm. Orange asterisks indicate TIMED/SEE Version 8 Level 3 data for 2002 and 2003. Version 8 data is not available for 2008. Black lines indicate TIMED/SEE Version 9 Level three data. Green pluses indicate the HEUVAC model spectra. Blue diamonds indicate the FISM model spectra. Red asterisks indicate data from the April 14, 2008 calibration rocket.

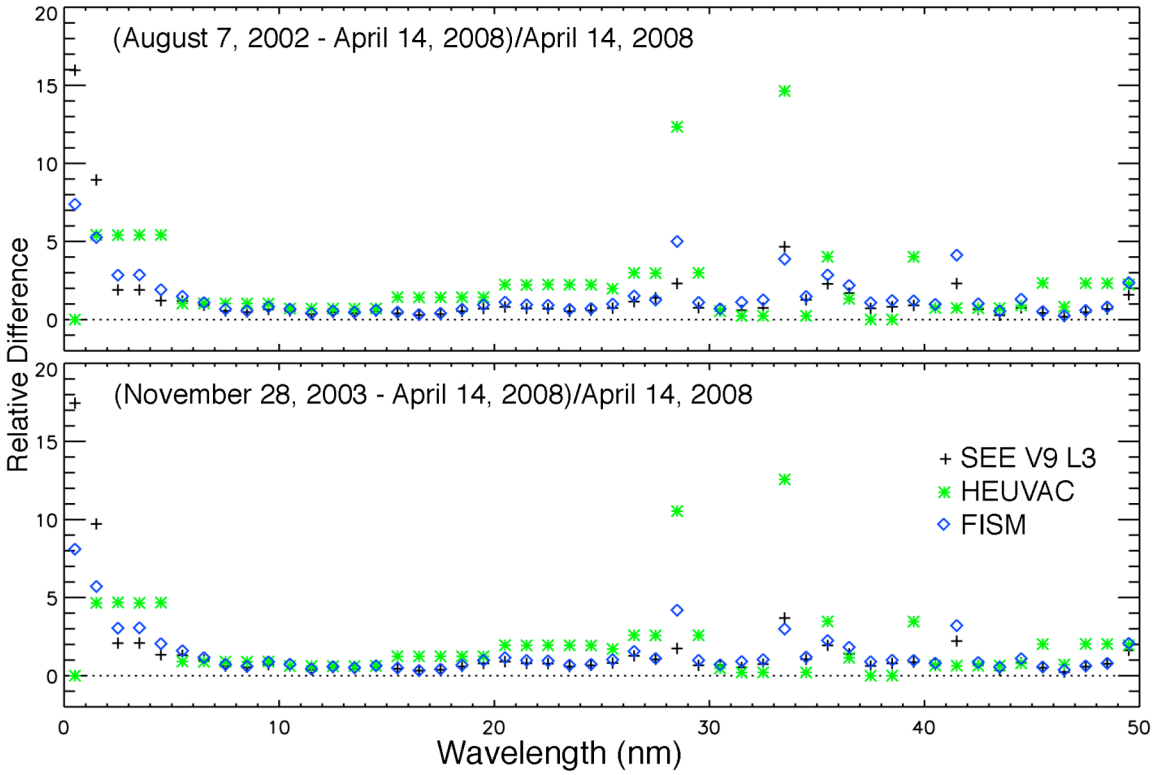

Figure 10: Relative difference in solar irradiance spectra for the dates indicated. Black + 's are from the TIMED/SEE Version 9 Level 3 data. Green *s are from the HEUVAC model. Blue diamonds are from the FISM model derived from SEE Version 9 data.

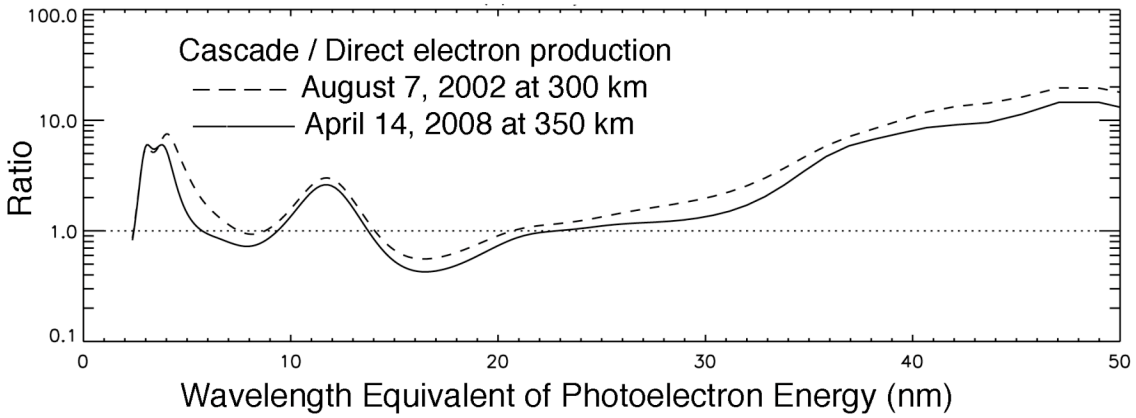

Figure 11: Ratio of cascade to direct photoelectron production as a function of the wavelength equivalent of the photoelectron energy from the FLIP/HEUVAC model pair. Solid line: Data for April 14, 2008. Dashed line: Data for August 7, 2002.